11th World Congress on Computational Mechanics (WCCM XI)
5th European Conference on Computational Mechanics (ECCM V)
6th European Conference on Computational Fluid Dynamics (ECFD VI)
E. Oñate, J. Oliver and A. Huerta (Eds)

SIMULATING SOIL–BUILDING INTERACTION WITH A FEM/BEM APPROACH

DIMAS B. RIBEIRO* AND JOÃO B. PAIVA†

* Department of Structural and Geotecnical Engineering
Polytechnic School of the University of São Paulo
Av. Prof. Almeida Prado tv. 2, n. 83, 05508–070 São Paulo, SP, Brazil
e-mail: dimas.ribeiro@usp.br

†Department of Structural Engineering
Engineering School of São Carlos
University of São Paulo
Av. Trabalhador Sãocarlense, 400, 13566-590 S ao Carlos, SP, Brazil,
e-mail: paiva@sc.usp.br - Web page:
http://www.set.eesc.usp.br/portal/pt/docentes/119-joao-batista-de-paiva

Key words: Boundary Elements, Finite Elements, Soil-Structure Interaction, Building

Abstract. The objective of this paper is to present formulations developed by the authors for soil-building interaction analysis. The soil is modeled with the boundary element method as a layered solid infinite for radial directions. Cylindrical piles are modeled with the finite element method using one dimensional elements. The raft is also modeled with the FEM, but with two dimensional elements. The analysis is static and all materials are considered homogeneous, isotropic, elastic and with linear behavior. Kelvin fundamental solutions are used in the BEM and an alternative multi-region technique is employed. Infinite boundary elements are employed for the far field simulation, allowing computational cost reduction without compromising the result accuracy. In the one dimensional elements used for the piles, displacements and tractions along the shaft are approximated by polynomial functions. The triangular three-node FE employed for the raft is obtained by superposing plate and membrane effects, totalizing six degrees of freedom per node. For the FEM-BEM coupling, the BEM tractions are considered as nodal reactions between the contact surfaces. The coupling is established using equilibrium and compatibility equations, obtaining a single system of equations that represents the complete pile-raft-soil problem.

1 INTRODUCTION

Piled rafts involve complex soil-structure interaction effects that require previous studies to be correctly considered in the project. The basis of these studies has to be chosen

among many options available and each one of them implies on advantages and disadvantages, as described below.

When possible, a good choice is to employ analytical methods. When correctly programmed they give trustful results in little processing time. In reference [1], for example, a solution is presented for an axially loaded pile with a rectangular cross section and immersed in a layered isotropic domain. The main disadvantage of these solutions is that they suit only specific situations, so many researches keep developing new ones to include new problems. Other works that may be cited are [2, 3].

If analytical solutions cannot be used, one alternative would be a numerical approach. The developments [4] of the numerical methods in the latter years and its versatility made them attractive to many researchers. The finite element method (FEM) is still popular [5, 6, 7, 8], however has some disadvantages when compared to other options such as the boundary element method (BEM). The FEM require the discretization of the domain, which has to be simulated as infinite in most soil-structure interaction problems. This implies on a high number of elements, leading to a large and sometimes impracticable processing time.

It becomes more viable solving these problems with the BEM, once only the boundary of the domains involved is discretized. This allows reducing the problem dimension, implying on less processing time. This advantage is explored in several works [9, 10, 11, 12, 13, 14, 15, 16] and new developments are making the BEM even more attractive to future applications. One is simulating non-homogeneous domains using an alternative multi-domain BEM technique [17], another is using mapping functions to make boundary elements infinite [18].

The objective of this paper is to present a formulation for building-soil interaction analysis that uses recent developments accomplished by the authors in references [17, 18]. The proposed formulation is applied into two examples. In the first, a squared raft resting on an infinite layered domain is considered. Results are compared with other formulations available in the literature including an analytical approach and good agreement is observed. The objective of the second example is to show all functionalities of the proposed formulation, considering a complete building interacting with a layered soil. No comparison with other authors is presented, nevertheless the results obtained may be considered coherent. Finally, it is concluded that the presented formulation may be considered a practical and attractive alternative in the field of soil-structure interaction simulation.

2 BOUNDARY ELEMENT FORMULATION

The equilibrium of a solid body can be represented by a boundary integral equation called the Somigliana Identity, which for homogeneous, isotropic and linear-elastic domains is

$$c_{ij}\left(y\right)u_j\left(y\right)+\int_{\Gamma}p^*_{ij}\left(x,y\right)u_j\left(x\right)d\Gamma\left(x\right)=\int_{\Gamma}u^*_{ij}\left(x,y\right)p_j\left(x\right)d\Gamma\left(x\right) \tag{1}$$

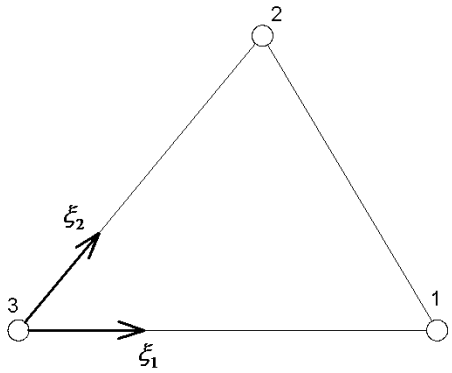

Figure 1: Triangular boundary element.

Equation (1) is written for a source point y at the boundary, where the displacement is $u_j(y)$. The constant c_{ij} depends on the Poisson ratio and the boundary geometry at y, as pointed out in reference [20]. The field point x goes through the whole boundary Γ, where displacements are $u_j(x)$ and tractions are $p_j(x)$. The integral kernels $u^*_{ij}(x,y)$ and $p^*_{ij}(x,y)$ are Kelvin three-dimensional fundamental solutions for displacements and tractions, respectively. Kernel $u^*_{ij}(x,y)$ has order $1/r$ and kernel $p^*_{ij}(x,y)$ order $1/r^2$, where $r = |x-y|$, so the integrals have singularity problems when x approaches y. Therefore the stronger singular integral, over the traction kernel, has to be defined in terms of a Cauchy Principal Value (CPV).

To solve Equation (1) numerically, the boundary is divided into regions within which displacements and tractions are approximated by known shape functions. Here these regions are of two types, finite boundary elements (BEs) and infinite boundary elements (IBEs). The BEs employed are triangular, as shown in Figure 1 with the local system of coordinates, $\xi_1\xi_2$, and the local node numbering. The following approximations are used for this BE:

$$u_j = \sum_{k=1}^{3} N^k u_j^k, \quad p_j = \sum_{k=1}^{3} N^k p_j^k \tag{2}$$

Equation (2) relates the boundary values u_j and p_j to the nodal values of the BE. The BEs have 3 nodes and for each node there are three components of displacement u_j^k and traction p_j^k. The shape functions N^k used for these approximations are

$$N^1 = \xi_1, \quad N^2 = \xi_2, \quad N^3 = 1 - \xi_1 - \xi_2 \tag{3}$$

The same shape functions are used to approximate the boundary geometry:

$$x_j = \sum_{k=1}^{3} N^k x_j^k \tag{4}$$

where x_j^k are the node coordinates. The same functions are also used to interpolate displacements and tractions for the IBEs:

$$u_j = \sum_{k=1}^{Np} N^k u_j^k, \quad p_j = \sum_{k=1}^{Np} N^k p_j^k \tag{5}$$

Each IBE has Np nodes and not the 3 that the BEs have. The IBE geometry, on the other hand, is approximated by special mapping functions, as discussed in more detail in Section 3.

By substituting Equations (2) and (5) in (1), Equation (6) is obtained:

$$\begin{gathered} c_{ij}(y)\, u_j(y) + \sum_{e=1}^{N_{BE}} \left\{ \sum_{k=1}^{3} \left[\Delta p_{ij}^{ek} u_j^k \right] \right\} + \sum_{e=1}^{N_{IBE}} \left\{ \sum_{k=1}^{Np} \left[\Delta^{\infty} p_{ij}^{ek} u_j^k \right] \right\} = \\ \sum_{e=1}^{N_{BE}} \left\{ \sum_{k=1}^{3} \left[\Delta u_{ij}^{ek} p_j^k \right] \right\} + \sum_{e=1}^{N_{IBE}} \left\{ \sum_{k=1}^{Np} \left[\Delta^{\infty} u_{ij}^{ek} p_j^k \right] \right\} \end{gathered} \tag{6}$$

N_{BE} is the number of BEs and N_{IBE} is the number of IBEs. For BEs:

$$\Delta p_{ij}^{ek} = \int_{\gamma_e} |J|\, N^k p_{ij}^*(x,y)\, d\gamma_e, \qquad \Delta u_{ij}^{ek} = \int_{\gamma_e} |J|\, N^k u_{ij}^*(x,y)\, d\gamma_e \tag{7}$$

In Equation (7), γ_e represents the domain of element e in the local coordinate system and the global system of coordinates is transformed to the local one by the Jacobian $|J| = 2A$, where A is the element area in the global system. On the other hand, for IBEs:

$$\Delta^{\infty} p_{ij}^{ek} = \int_{\gamma_e} |^{\infty}J|\, N^k p_{ij}^*(x,y)\, d\gamma_e, \qquad \Delta^{\infty} u_{ij}^{ek} = \int_{\gamma_e} |^{\infty}J|\, N^k u_{ij}^*(x,y)\, d\gamma_e \tag{8}$$

Equation (8) is analogous to (7), and the calculation of Jacobian $|^{\infty}J|$ is discussed in Section 3. Integrals of Equations (7) and (8) are calculated by standard BEM techniques. Non-singular integrals are evaluated numerically by using integration points. The singular ones, on the other hand, are evaluated by the technique presented in reference [19]. Finally, the free term c_{ij} may be obtained by rigid body motions. Writing Equation (6) for all boundary nodes leads to the following system:

$$\Delta p \cdot u = \Delta u \cdot p \tag{9}$$

The Δp_{ij}^{ek} and $\Delta^{\infty} p_{ij}^{ek}$ element contributions, including the free term c_{ij}, are assembled into matrix Δp, while Δu_{ij}^{ek} and $\Delta^{\infty} u_{ij}^{ek}$ contributions are assembled into matrix Δu. Vectors u and p contain all boundary displacements and tractions, respectively. Reorganizing this system so as to separate the known boundary values from the unknown yields a system of equations whose solution is all the unknown boundary values.

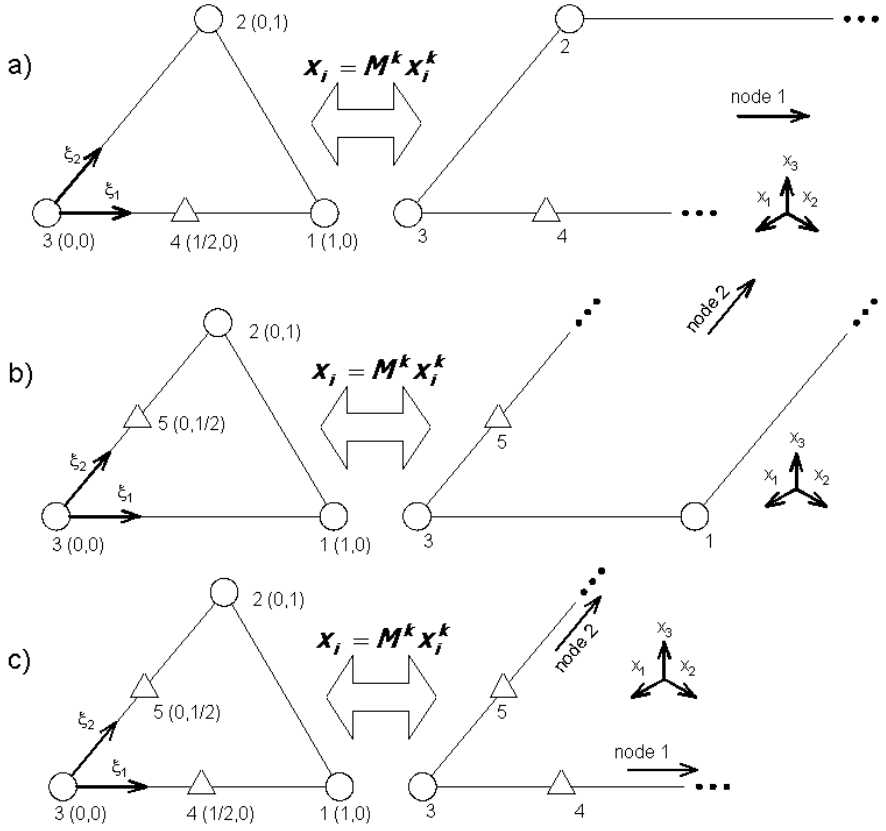

Figure 2: Types of mapping.

3 INFINITE BOUNDARY ELEMENTS

Three types of mapping are considered, as illustrated in Figure 2.

In the first type, represented in Figure 2a, only direction ξ_1 is mapped to infinity and node 1 is placed at infinity. The IBE is represented in the local coordinate system on the left and in the global coordinate system on the right. The global coordinates x_i are related to the local ones by special mapping functions, M^k, and the nodal global coordinates, x_i^k. Node 4 is created only to replace node 1 in the mapping and does not contribute to the integrals.

Figure 2b is analogous to Figure 2a, but in this case only direction ξ_2 is mapped to infinity and node 2 is placed at infinity. Therefore, node 5 is created to facilitate the mapping. Finally, in Figure 2c both local directions are mapped to infinity and nodes 1 and 2 are placed at infinity. As a result, the auxiliary nodes 4 and 5 must be created to replace them in the mapping.

In reference [18], auxiliary coordinates $\bar{\xi}_1$ and $\bar{\xi}_2$ are used to obtain the mapping functions for each case. When only direction ξ_1 is mapped to infinity, the result is:

$$M_{1\infty}^4 = \bar{\xi}_1(\xi_1) = \frac{\xi_1}{1-\xi_1} \tag{10}$$

$$M_{1\infty}^2 = \xi_2 \tag{11}$$

$$M_{1\infty}^3 = 1 - \bar{\xi}_1(\xi_1) - \xi_2 = 1 - \frac{\xi_1}{1-\xi_1} - \xi_2 \tag{12}$$

The symbol "1∞" is used to indicate that these expressions are valid if only direction ξ_1 is mapped to infinity. These functions are then employed to relate the local system of coordinates to the global one. In other words:

$$x_i = M_{1\infty}^4 x_i^4 + M_{1\infty}^2 x_i^2 + M_{1\infty}^3 x_i^3 \tag{13}$$

After obtaining Equation (13), the Jacobian used when only direction ξ_1 is mapped to infinity may be calculated as follows:

$$|^{\infty}J_1| = \frac{\partial x_1}{\partial \xi_1}\frac{\partial x_2}{\partial \xi_2} - \frac{\partial x_2}{\partial \xi_1}\frac{\partial x_1}{\partial \xi_2} = \frac{2A_1}{(1-\xi_1)^2} \tag{14}$$

where A_1 is the area of the triangle drawn between nodes 2, 3 and 4 in the global system of coordinates.

For mapping only in direction ξ_2 to infinity, the functions obtained are:

$$M_{2\infty}^1 = \xi_1 \tag{15}$$

$$M_{2\infty}^5 = \bar{\xi}_2(\xi_2) = \frac{\xi_2}{1-\xi_2} \tag{16}$$

$$M_{2\infty}^{3} = 1 - \xi_1 - \bar{\xi}_2\left(\xi_2\right) = 1 - \xi_1 - \frac{\xi_2}{1-\xi_2} \tag{17}$$

The symbol "2∞" is used to indicate that only direction ξ_2 is mapped to infinity. Therefore, the global system is related to the local one as follows:

$$x_i = M_{2\infty}^{1} x_i^1 + M_{2\infty}^{5} x_i^5 + M_{2\infty}^{3} x_i^3 \tag{18}$$

and the Jacobian is

$$|^{\infty} J_2| = \frac{2A_2}{\left(1-\xi_2\right)^2} \tag{19}$$

where A_2 refers to the area of the triangle drawn between nodes 1, 3 and 5 in the global system of coordinates.

Finally, for mapping in both directions ξ_1 and ξ_2 to infinity, the mapping functions are

$$M_{\infty}^{4} = \frac{\xi_1}{1-\xi_1} \tag{20}$$

$$M_{\infty}^{5} = \frac{\xi_2}{1-\xi_2} \tag{21}$$

$$M_{\infty}^{3} = 1 - \frac{\xi_1}{1-\xi_1} - \frac{\xi_2}{1-\xi_2} \tag{22}$$

The symbol "∞" is used to indicate that both directions are mapped to infinity. The local system of coordinates is related to the global one as follows:

$$x_i = M_{\infty}^{4} x_i^4 + M_{\infty}^{5} x_i^5 + M_{\infty}^{3} x_i^3 \tag{23}$$

and the Jacobian is now

$$|^{\infty} J_3| = \frac{2A_3}{\left(1-\xi_1\right)^2\left(1-\xi_2\right)^2} \tag{24}$$

where A_3 is the area of the triangle drawn between nodes 3, 4 and 5 in the global system.

4 LOAD LINES IN THE SOIL

In this work, the reactive tractions from the piles are applied in the soil as load lines. Figure 3 presents the model adopted, with four nodes equally spaced along the pile.

The load lines influence may be computed in Equation (1) with an additional term as follows

$$\begin{gathered} \mathrm{c_{ij}}\left(y\right) u_j\left(y\right) + \int_{\Gamma} p_{ij}^{*}\left(x,y\right) u_j\left(x\right) d\Gamma\left(x\right) = \\ \int_{\Gamma} u_{ij}^{*}\left(x,y\right) p_j\left(x\right) d\Gamma\left(x\right) + \sum_{e=1}^{nl}\left[\int_{\Gamma^e} u_{ij}^{*}\left(x,y\right) s_j^e\left(x\right) d\Gamma^e\left(x\right)\right] \end{gathered} \tag{25}$$

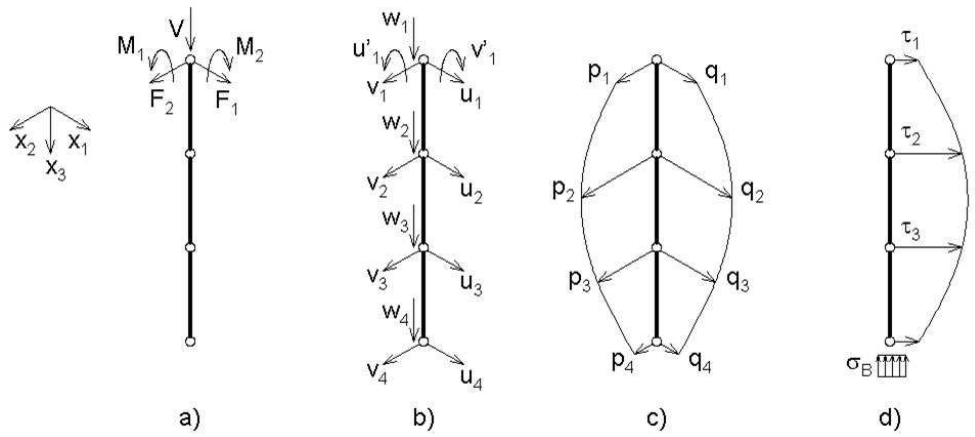

Figure 3: Model for load lines.

where nl is the number of load lines, Γ^e are their external surface and s_j^e are the tractions presented in Figures 3c and 3d. The tractions are approximated from the nodal values s_j^{ek} using nf polynomial shape functions ϕ:

$$s_j^e = \sum_{k=1}^{nf} \phi^k s_j^{ek} \tag{26}$$

Shape functions are written with a dimensionless coordinate $\xi = {}^{2x_3}/_{L} - 1$, where L is the load line length and x_3 is the vertical global coordinate. One may observe that $-1 \leq \xi \leq 1$, so the use of Gauss points is facilitated. For the horizontal tractions, illustrated in Figure 3c, $nf = 4$ and the shape functions are:

$$\begin{aligned} \phi^1 &= \tfrac{1}{16}\left(-9\xi^3 + 9\xi^2 + \xi - 1\right), \quad \phi^2 = \tfrac{1}{16}\left(27\xi^3 - 9\xi^2 - 27\xi + 9\right), \\ \phi^3 &= \tfrac{1}{16}\left(-27\xi^3 - 9\xi^2 + 27\xi + 9\right), \quad \phi^4 = \tfrac{1}{16}\left(9\xi^3 + 9\xi^2 - \xi - 1\right) \end{aligned} \tag{27}$$

For shear tractions in direction x_3, $nf = 3$ and the shape functions are

$$\phi^1 = \frac{1}{8}\left(9\xi^2 - 1\right), \quad \phi^2 = \frac{1}{4}\left(-9\xi^2 - 6\xi + 3\right), \quad \phi^3 = \frac{1}{8}\left(9\xi^2 + 12\xi + 3\right) \tag{28}$$

Finally, for the base reaction $nf = 1$ and a constant approximation is used. Using the shape functions presented above, the integrals that are not singular may be numerically calculated using Gauss points. The term referent to the load lines becomes singular only when the source point belongs to a load line base which is being integrated. In this case, the integral calculation is analytical.

Writing Equation (28) for all boundary points plus the points defined on each load line, the following system of equations is obtained:

$$[H]\{u\} = [G]\{p\} - [M]\{s\} \tag{29}$$

Matrix $[M]$ is obtained from the integrals calculated for all load lines, and vector $\{s\}$ contains the tractions prescribed for them. As the number of equations is equal to the number of unknowns, the system may be solved obtaining all unknowns.

5 FEM-BEM COUPLING

Each pile is modeled using a single finite element with polynomial shape functions. Lateral displacements are approximated using fourth degree polynomials $\{\varphi\}$. Vertical displacements and lateral tractions are approximated using third degree polynomials $\{\phi\}$. Vertical tractions are approximated using second degree polynomials $\{\omega\}$ and the tractions at the pile base are considered constant. Using a dimensionless coordinate $\xi = \frac{x_3}{L}$, where x_3 is the global vertical coordinate and L is the pile length, $\{\varphi\}$, $\{\phi\}$ and $\{\omega\}$ may be written as:

$$\{\varphi\} = \begin{Bmatrix} -\frac{99}{4}\xi^4 + 45\xi^3 - \frac{85}{4}\xi^2 + 1 \\ -\frac{9}{2}\xi^4 L + 9\xi^3 L - \frac{11}{2}\xi^2 L + \xi L \\ \frac{81}{2}\xi^4 - \frac{135}{2}\xi^3 + 27\xi^2 \\ -\frac{81}{4}\xi^4 + 27\xi^3 - \frac{27}{4}\xi^2 \\ \frac{9}{2}\xi^4 - \frac{9}{2}\xi^3 + \xi^2 \end{Bmatrix} \tag{30}$$

$$\{\phi\} = \begin{Bmatrix} -\frac{9}{2}\xi^3 + 9\xi^2 - \frac{11}{2}\xi + 1 \\ \frac{27}{2}\xi^3 - \frac{45}{2}\xi^2 + 9\xi \\ -\frac{27}{2}\xi^3 + 18\xi^2 - \frac{9}{2}\xi \\ \frac{9}{2}\xi^3 - \frac{9}{2}\xi^2 + \xi \end{Bmatrix} \tag{31}$$

$$\{\omega\} = \begin{Bmatrix} \frac{9}{2}\xi^2 - \frac{9}{2}\xi + 1 \\ -9\xi^2 + 6\xi \\ \frac{9}{2}\xi^2 - \frac{3}{2}\xi \end{Bmatrix} \tag{32}$$

The next step is obtaining the total potential energy function, considering internal and external contributions. To obtain the final system of equations, such function must be minimized with respect to the nodal parameters. The result is:

$$[K]\{u\} = \{f\} - [Q]\{y\} \rightarrow [K]\{u\} = \{f\} - \{r\} \tag{33}$$

where $[K]$ is the stiffness matrix of the pile, $\{u\}$ contains nodal displacements, $\{f\}$ contains nodal loads, $\{y\}$ contains distributed tractions and $[Q]$ is a matrix that transforms distributed tractions into nodal loads. Therefore, $\{r\}$ contains nodal loads that represent the distributed loads.

Now a brief description of the triangular finite element used for the raft and slabs will be presented. The element has three nodes at its vertices as presented in Figure 4a with

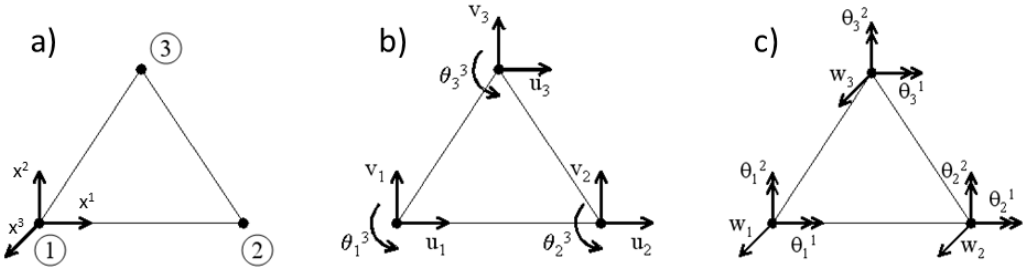

Figure 4: Triangular finite element.

the local node numbering and a local rectangular system of coordinates x^i, where the superscript i indicates the direction. Each node, indicated with the subscript j, has six degrees of freedom (DOFs). Three of them, u_j, v_j and θ_j^3, may be visualized in Figure 4b which refers to the membrane effects. The other three, w_j, θ_j^1 and θ_j^2, are presented in Figure 4c which refers to the plate effects. In Figure 4c, rotational DOFs are indicated with a double arrow for better visualization. All DOFs of the finite element may be arranged into three vectors, one for each node, as shown below:

$$\begin{aligned}
\{\mathbf{u}_1\}^T &= \left\{ \begin{array}{cccccc} u_1 & v_1 & {\theta_1}^3 & w_1 & {\theta_1}^1 & {\theta_1}^2 \end{array} \right\} \\
\{\mathbf{u}_2\}^T &= \left\{ \begin{array}{cccccc} u_2 & v_2 & {\theta_2}^3 & w_2 & {\theta_2}^1 & {\theta_2}^2 \end{array} \right\} \\
\{\mathbf{u}_3\}^T &= \left\{ \begin{array}{cccccc} u_3 & v_3 & {\theta_3}^3 & w_3 & {\theta_3}^1 & {\theta_3}^2 \end{array} \right\}
\end{aligned} \tag{34}$$

Displacements at any point P of the finite element, with coordinates x_1, x_2 and x_3, may be written as

$$\{\mathbf{u}\} = \left\{ \begin{array}{c} u \\ v \\ w \end{array} \right\} = \left\{ \begin{array}{c} u_0 - x_3 \frac{\partial w_0}{\partial x_1} \\ v_0 - x_3 \frac{\partial w_0}{\partial x_2} \\ w_0 \end{array} \right\} \tag{35}$$

where u_0, v_0, and w_0 are the displacements for the projection of P at the mid plane of the finite element. The strain field may be obtained from the displacements as follows:

$$\{\varepsilon\} = \{\varepsilon_m\} + \{\varepsilon_p\} = \left\{ \begin{array}{c} \frac{\partial u_0}{\partial x_1} \\ \frac{\partial v_0}{\partial x_2} \\ \frac{\partial u_0}{\partial x_2} + \frac{\partial v_0}{\partial x_1} \end{array} \right\} - x_3 \left\{ \begin{array}{c} \frac{\partial^2 w_0}{\partial {x_1}^2} \\ \frac{\partial^2 w_0}{\partial {x_2}^2} \\ 2\frac{\partial^2 w_0}{\partial x_1 \partial x_2} \end{array} \right\} \tag{36}$$

where index m corresponds to the membrane effect and the index p indicates the plate effect. Equation (36) relates the strain field to the displacement field, which may be related to the nodal displacements using the element shape functions. Using these functions and Equation (36), it is possible to relate strains with the DOFs of the finite element as follows:

$$\{\varepsilon\} = [B] \left\{ \begin{array}{c} \mathbf{u}_1 \\ \mathbf{u}_2 \\ \mathbf{u}_3 \end{array} \right\} \tag{37}$$

It is also necessary to relate strains with stresses. For linear elasticity this may be done using a matrix $[D]$ which is obtained from Hooke's law:

$$\{\sigma\} = [D]\{\varepsilon\} \tag{38}$$

In the end, the stiffness matrix of the element is obtained by integrating the domain Ω of the element:

$$[K] = \int_{\Omega} [B]^T [D][B]\, d\Omega \tag{39}$$

More detail about the membrane and plate effects of this element may be consulted in references [21, 22], respectively.

All finite element contributions, including piles and the raft, are assembled to the same system of equations. This system has the form of Equation (33), which is later used to demonstrate how the FEM/BEM coupling is made. The starting point is Equation (29), which may be rewritten as:

$$[H]\{u\} = [T]\{y\} \tag{40}$$

Matrix $[T]$ contains the terms of matrices $[G]$ and $[M]$ and $\{y\}$ contains the distributed loads of vectors $\{p\}$ and $\{s\}$. Next step is isolating the distributed loads, which are transformed in nodal loads using a matrix $[Q]$.

$$[T]^{-1}[H]\{u\} = \{y\} \rightarrow [B]\{u\} = \{y\} \tag{41}$$

$$[Q][B]\{u\} = [Q]\{y\} \rightarrow [D]\{u\} = \{r\} \tag{42}$$

Before relating Equations (33) and (42), they must be expanded as to contain all degrees of freedom defined in the coupled FEM-BEM model. The result is

$$\left[\bar{K}\right]\{\bar{u}_{FEM}\} = \left\{\bar{f}\right\} - \{\bar{r}_{FEM}\}, \quad \left[\bar{D}\right]\{\bar{u}_{BEM}\} = \{\bar{r}_{BEM}\} \tag{43}$$

These equations are related by imposing compatibility and equilibrium conditions, which are $\{\bar{u}_{FEM}\} = \{\bar{u}_{BEM}\} = \{\bar{u}\}$ and $\{\bar{r}_{FEM}\} = \{\bar{r}_{BEM}\} = \{\bar{r}\}$. The following expression is then obtained:

$$\left[\bar{K}\right]\{\bar{u}\} = \left\{\bar{f}\right\} - \left[\bar{D}\right]\{\bar{u}\} \rightarrow \left(\left[\bar{K}\right] - \left[\bar{D}\right]\right)\{\bar{u}\} = \left\{\bar{f}\right\} \rightarrow \left[\bar{A}\right]\{\bar{u}\} = \left\{\bar{f}\right\} \tag{44}$$

where $\{\bar{u}\}$ contain all unknown displacements of the FEM-BEM model. Once the number of equations is equal to the number of unknowns, the system may be solved obtaining all unknowns.

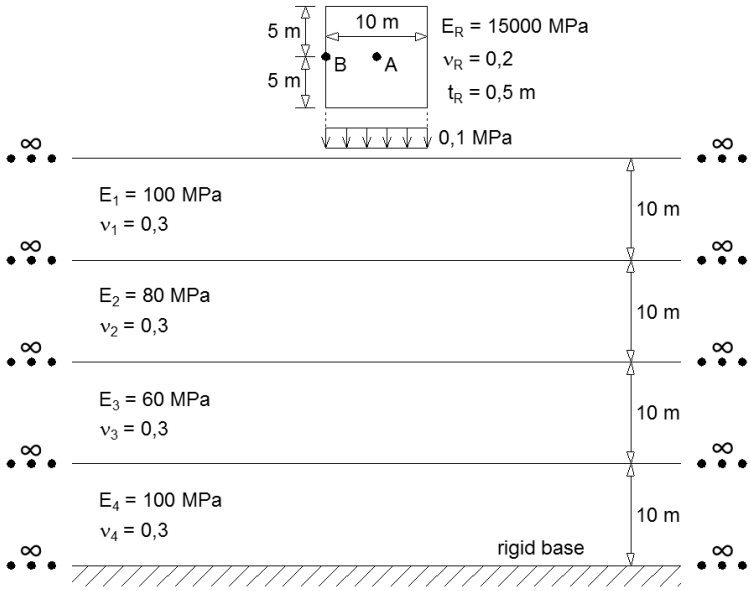

Figure 5: First example.

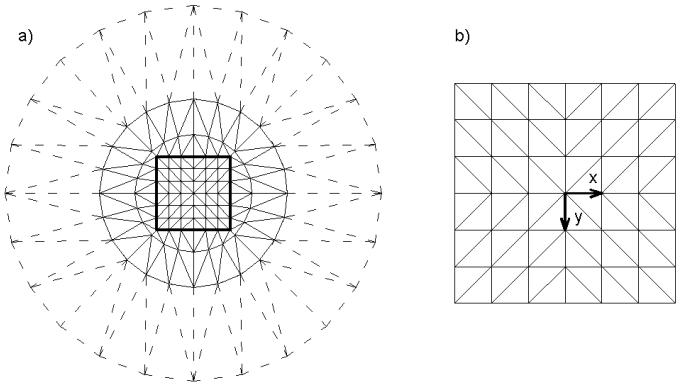

Figure 6: Mesh employed.

6 EXAMPLES

6.1 Raft on a layered domain

Here a squared raft over a domain with 4 layers is considered, as presented in Figure 5 with all geometrical and material parameters. Young's module and Poisson ratio are named E and ν, respectively, while thickness is indicated as t. The subscript R is used for the raft and numbers are used for the layers. Point A is at the center of the raft, point B is at the side midpoint and an uniform $0,1\ MPa$ load is applied over it.

Figure 6 presents the mesh. The mesh for the surface and contacts between layers is presented in Figure 6a, where dashed lines represent 48 IBEs and other ones represent 168 BEs. Figure 6b presents the 72 FE mesh employed for the raft with an xy system of coordinates.

Displacements obtained for points A and B are presented in Table 1 with results obtained by other authors. Good agreement may be observed. To complement this example, the bending moment for axis x was calculated. The values obtained for points A and B were, respectively, $3,83 \times 10^{-2}\ kNm/m$ and $2,20 \times 10^{-2}\ kNm/m$.

	$d_A\ (cm)$	$d_B\ (cm)$
This work	$0,97$	$0,74$
[23]	$1,07$	$0,78$
[24]	$1,14$	$0,87$
[25]	$1,20$	$0,89$

Table 1: Vertical displacements

6.2 Building resting on a layered domain

The objective of this example is to demonstrate the generality of the presented formulation. The problem to be analyzed is presented in Figure 7 and considers a building with its foundations, resting on a layered media. In Figure 7a the lateral view is illustrated, Figure 7b contains the standard floor considered and in Figure 7c is presented the top view of the structural foundations included.

The Poisson Ratio is zero for all soil layers. The elasticity modulus of the layers is 60 MPa for the top one, 80 MPa for the second and 90000 MPa for the base layer. The thickness is 15 m for the top layer, 20 m for the second and the base layer is considered infinite. The diameter of all piles is $0,5\ m$, their length is 10 m and they are spaced of 5 m. The square raft has size 20 m and thickness $0,5\ m$. The elasticity modulus of all materials modeled with the FEM is 15000 MPa and their Poisson ratio is $0,2$. This includes all piles, beams, columns, slabs and the raft.

The building has four floors, as shown in Figure 7a. All floors have the same standard geometry, as presented in Figure 7b, with a slab with thickness $0,3\ m$, four beams supporting this slab and four columns supporting the beams. A square cross section size 1

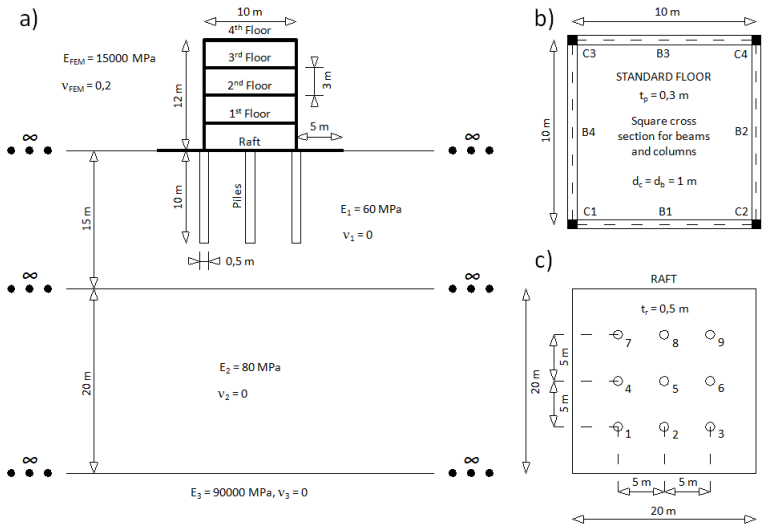

Figure 7: Soil-building interaction

m is used for all beams and columns. The base of each column is connected to the raft at the same node where a corner pile is connected. Corner piles are numerated in Figure 7c as 1, 3, 7 and 9.

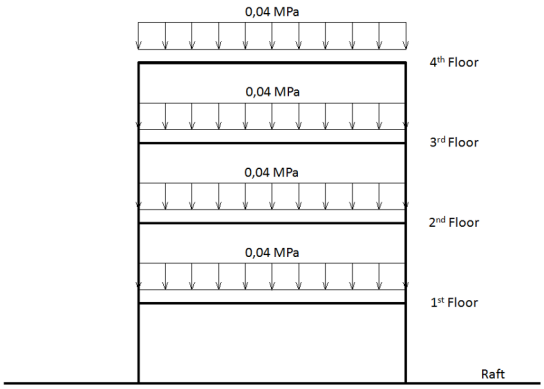

Figure 8: Vertical loads applied

The loads considered are vertical and presented in Figure 8. They are uniformly distributed over the slabs, with an intensity of $0,04\ MPa$.

Figure 9 presents the FE-BE-IBE mesh employed in the example. Figure 9a contains the top view of the mesh used for the soil surface and contacts between layers, totalizing 480 BEs and 96 IBEs. The square detached at the center indicates the position of the raft at the surface. In Figure 9b is illustrated the mesh with 32 FEs used for the raft, together with the position of the piles. Finally, Figure 9c contains the 32 FE mesh used for the slabs. Lines detached at the boundary indicate the FEs used for beams, totalizing

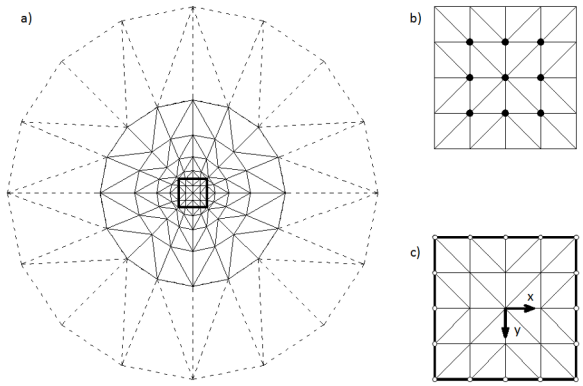

Figure 9: FE/BE/IBE mesh employed

16 FEs for each floor. Furthermore, each part of the columns between floors is divided into 4 FEs. Considering all floors plus the raft, the total number of two-dimensional FEs is 160 and the total of one-dimensional FEs is 128.

Piles are also simulated with the FEM, employing the FE with 14 parameters presented previously. The axis of any pile is orthogonal to the surface of the soil.

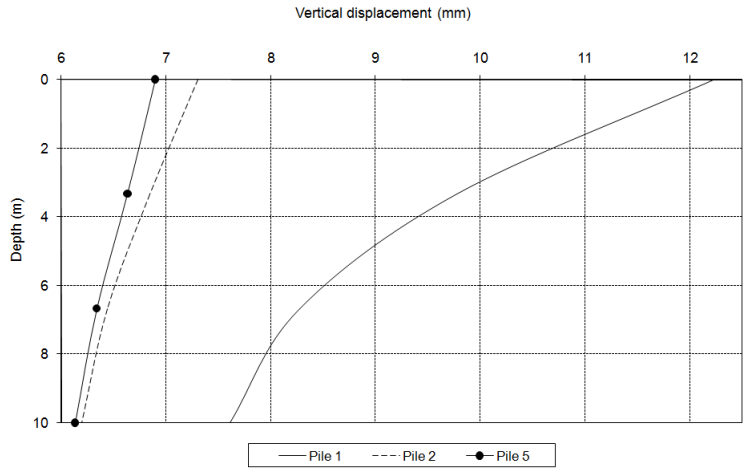

Figure 10: Vertical displacement at slabs

The vertical displacements along the axis of the piles are shown in Figure 10. Only piles number 1, 2 and 5 are presented (see Figure 7c) because the results are symmetric for the other ones. Piles placed at corners presented higher displacements, with the value of $12,2\ mm$ at the top. This result may be considered coherent because the base of the columns of the building is placed exactly over the corner piles. The vertical displacement obtained at the top of pile 2 was $7,3\ mm$ and for pile 5 it was $6,9\ mm$.

Figure 11 contains results calculated for the fourth floor, as numbered in Figure 7a. Values are evaluated along a diagonal line on the floor, which extremes are placed at

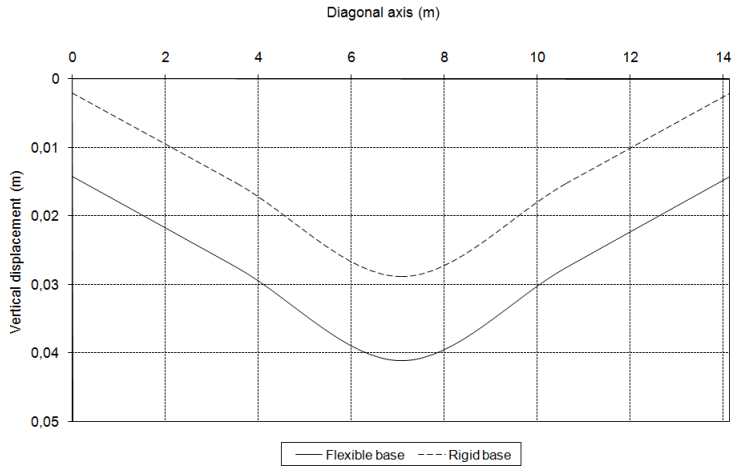

Figure 11: Vertical displacement at the fourth floor

columns $C1$ and $C4$, as shown in Figure 7b. Two results are presented. One is considering the elastic foundation presented in Figure 7a and the other is considering a rigid base. For the rigid base, displacements at the base of the columns are simply restrained. It may be observed that the vertical displacements of the slab are significantly higher when an elastic base is considered, what may be considered a predictable result. The maximum displacement at the slab for a rigid base is $28,8\ mm$ and for an elastic foundation it is $41,0\ mm$.

7 CONCLUSIONS

In this paper a formulation for building-soil interaction analysis was presented. The FEM/BEM equations together with the techniques from references [17, 18] contributed with reducing the total number of degrees of freedom. Piles are modeled using one-dimensional FEs, whose influence in the soil is computed by integrating load lines. Two examples were presented. On the first one the values obtained were compared with other publications and good agreement was observed. On the second one no comparison was presented, nevertheless the results obtained were considered coherent. In the end, it may be concluded that the presented formulation is a powerful and attractive alternative for soil-structure interaction analysis.

Acknowledgements

Thanks are due to the research council FAPESP and the University of São Paulo.

REFERENCES

[1] Basu, D., Prezzi, M., Salgado, R. and Chakraborty, T. Settlement analysis of piles with rectangular cross sections in multi-layered soils, *Comput. Geotech.* (2008)

35:563–575.

[2] Shahmohamadi, M., Khojasteh, A., Rahimian, M. and Pak, R.Y.S. Axial soil-pile interaction in a transversely isotropic half-space, *Int. J. Eng. Sci.* (2011) **49**:934–949.

[3] Georgiadis, K., Georgiadis, M. and Anagnostopoulos, C. Lateral bearing capacity of rigid piles near clay slopes, *Soils. Found.* (2013) **53**:144–154.

[4] Clouteau, D., Cottereau, R. and Lombaert, G. Dynamics of structures coupled with elastic media - A review of numerical models and methods, *J. Sound Vib.* (2013) **332**:2415–2436.

[5] Kim, Y. and Jeong, S. Analysis of soil resistance on laterally loaded piles based on 3D soilpile interaction, *Comput. Geotech.* (2011) **38**:248–257.

[6] Bourgeois, E., de Buhan, P. and Hassen, G. Settlement analysis of piled-raft foundations by means of a multiphase model accounting for soil-pile interactions, *Comput. Geotech.* (2012) **46**:26–38.

[7] Su, D. and Li, J.H. Three-dimensional finite element study of a single pile response to multidirectional lateral loadings incorporating the simplified state-dependent dilatancy model, *Comput. Geotech.* (2013) **50**:129–142.

[8] Peng, J.R., Rouainia, M. and Clarke, B.G. Finite element analysis of laterally loaded fin piles, *Comput. Struct.* (2010) **88**:1239–1247.

[9] Ai, Z.Y. and Cheng, Y.C. Analysis of vertically loaded piles in multi-layered transversely isotropic soils by BEM, *Eng. Anal. Bound. Elem.* (2013) **37**:327–335.

[10] Matos Filho, R., Mendonça, A.V. and Paiva, J.B. Static boundary element analysis of piles submitted to horizontal and vertical loads, *Eng. Anal. Bound. Elem.* (2005) **29**:195–203.

[11] Masoumi, H.R., Degrande, G. and Lombaer, G. Prediction of free field vibrations due to pile driving using a dynamic soilstructure interaction formulation, *Soil Dyn. Earthq. Eng.* (2007) **27**:126–143.

[12] Padron, L.A., Aznarez, J.J. and Maeso O. 3-D boundary elementfinite element method for the dynamic analysis of piled buildings, *Eng. Anal. Bound. Elem.* (2011) **35**:465–477.

[13] Almeida, V.S. and Paiva, J.B. Static analysis of soil/pile interaction in layered soil by BEM/BEM coupling, *Adv. Eng. Softw.* (2007) **38**:835–845.

[14] Millan, M.A. and Dominguez, J. Simplified BEM/FEM model for dynamic analysis of structures on pile sand pile groups in viscoelastic and poroelastic soils, *Eng. Anal. Bound. Elem.* (2009) **33**:25–34.

[15] Elahi, H., Moradi, M., Poulos, H.G. and Ghalandarzadeh, A. Pseudostatic approach for seismic analysis of pile group, *Comput. Geotech.* (2010) **37**:25–39.

[16] Kucukarslan, S., Banerjee, P.K. and Bildik, N. Inelastic analysis of pile soil structure interaction, *Eng. Struct.* (2003) **25**:1231–1239.

[17] Ribeiro, D.B. and Paiva, J.B. An alternative multi-region BEM technique for three-dimensional elastic problems, *Eng. Anal. Bound. Elem.* (2009) **33**:499–507.

[18] Ribeiro, D.B. and Paiva, J.B. Analyzing static three-dimensional elastic domains with a new infinite boundary element formulation, *Eng. Anal. Bound. Elem.* (2010) **34**:707–713.

[19] Guiggiani, M. and Gigante, A. A general algorithm for multidimensional cauchy principal value integrals in the boundary element method, *J. Appl. Mech.* (1990) **57**:906–915.

[20] Moser, W., Duenser, C. and Beer, G. Mapped infinite elements for three-dimensional multi-region boundary element analysis, *Int. J. Numer. Meth. Eng.* (2004) **61**:317–328.

[21] Bergan, P.G. and Felippa, C.A. A triangular membrane element with rotacional degrees of freedom, *Comput. Method. Appl. M.* (1985) **50**:25–69.

[22] Batoz, J.L. A study of tree-node triangular plate bending elements, *Int. J. Numer. Meth. Eng.* (1980) **15**:1771–1812.

[23] Wardle, L.J. and Fraser, R.A. Finite element analysis of a plate on a layered cross-anisotropic foundation, in "Proceedings of the First International Conference of Finite Element Methods in Engineering" (1974) University of New South Wales, Australia, 565–578.

[24] Fraser, R.A. and Wardle, L.J. Numerical analysis of rectangular rafts on layered foundations, *Geotechnique* (1976) **26**:613–630.

[25] Wang, Y.H., Tham, L.G., Tsui, Y. and Yue, Z.Q. Plate on layered foundation analyzed by a semi-analytical and semi-numerical method, *Comput. Geotech.* (2003) **30**:409–418.